THE JOURNAL OF PHYSICAL CHEMISTRY B

Article

pubs.acs.org/JPCB

Molecular Dynamics Simulations of Tri-*n*-butyl-phosphate/*n*-Dodecane Mixture: Thermophysical Properties and Molecular Structure

Shengting Cui,*[,†] Valmor F. de Almeida,[‡] and Bamin Khomami*[,†]

[†]Materials Research and Innovation Laboratory Department of Chemical and Biomolecular Engineering, University of Tennessee, Knoxville, Tennessee 37996, United States

[‡]Chemical Sciences Division, Oak Ridge National Laboratory, Oak Ridge, Tennessee 37831, United States

Supporting Information

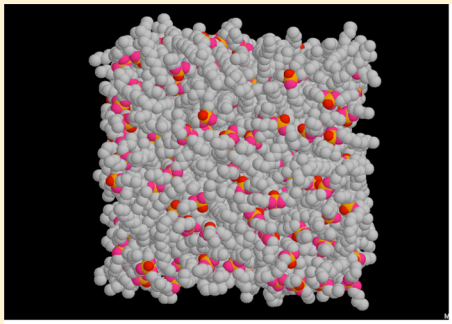

Snapshot for a 50/50 mixture

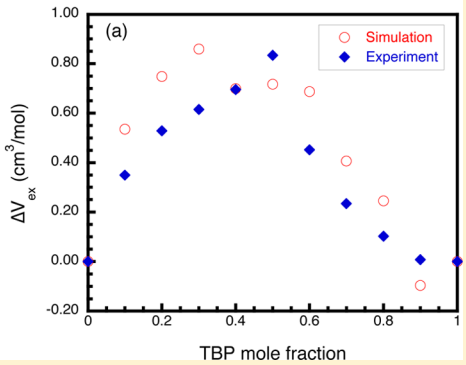

ABSTRACT: Molecular dynamics simulations of tri-*n*-butyl-phosphate (TBP)/*n*-dodecane mixture in the liquid phase have been carried out using two recently developed TBP force field models (*J. Phys. Chem. B* **2012**, *116*, 305) in combination with the all-atom optimized potentials for liquid simulations (OPLS-AA) force field model for *n*-dodecane. Specifically, the electric dipole moment of TBP, mass density of the mixture, and the excess volume of mixing were computed with TBP mole fraction ranging from 0 to 1. It is found that the aforementioned force field models accurately predict the mass density of the mixture in the entire mole fraction range. Commensurate with experimental measurements, the electric dipole moment of the TBP was found to slightly increase with the mole fraction of TBP in the mixture. Also, in accord with experimental data, the excess volume of mixing is positive in the entire mole fraction range, peaking at TBP mole fraction range 0.3−0.5. Finally, a close examination of the spatial pair correlation functions between TBP molecules, and between TBP and *n*-dodecane molecules, revealed formation of TBP dimers through self-association at close distance, a phenomenon with ample experimental evidence.

I. INTRODUCTION

Aqueous processes are widely used for separation and recovery of various elements or element groups from spent nuclear fuel.[1,2] The key feature of aqueous-based reprocessing technologies is the selective transfer of elements between aqueous and organic solution phases via solvent extraction in liquid−liquid contactor devices. Current liquid−liquid extraction systems for reprocessing of spent nuclear fuel use an aqueous phase, which contains the actinyl ions to be extracted, and an organic phase, consisting of a mixture of an extracting agent and a diluent. The most commonly used extracting agent is the tri-*n*-butyl-phosphate ester (TBP; Figure 1) with *n*-dodecane as the diluent.

This extraction method has been used to extract a variety of chemical species, including uranium,[3−6] plutonium,[7,8] zirconium,[9] and other metals.[2] With the current renewed interest in nuclear energy and waste management, there exists a need for efficient extraction and separation of different metallic cation species.[2,10−12] To this end, development of high-fidelity computational methods for predicting the thermophysical properties of the aforementioned liquid phases as well as elucidating the molecular mechanism involved in the extraction process has received increased attention. Reliable molecular level knowledge is particularly important in view of the complexity of the extraction physicochemical process and the

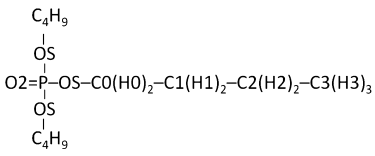

Figure 1. Schematic of TBP molecule.

Received: April 24, 2014
Revised: August 18, 2014
Published: August 19, 2014

   dx.doi.org/10.1021/jp5040135 | *J. Phys. Chem. B* 2014, 118, 10750−10760

lack of understanding of interfacial speciation. For example, the phenomenon of the third phase formation in the organic phase,[13−16] has practical and scientific importance for nuclear solvent extraction.

Many experimental measurements of thermophysical properties of TBP and related mixtures in the liquid phase were carried out in the early years of nuclear energy applications, e.g., dipole moment, diffusivity, and water solubility.[1] A recent study[11] systematically measured the mass density and viscosity of TBP bulk phase and its mixture with *n*-dodecane at various mole fractions, thus providing a reference for calibration of molecular models. The investigation of TBP and its mixture has led to the probing of molecular level behaviors. In particular, a variety of experiments,[17] such as, distribution coefficient experiments,[18] infrared spectroscopy,[19] nuclear magnetic resonance,[20] calorimetry,[21−25] and vapor pressure osmometry,[26,27] have been carried out to study the self-association of TBP molecules in the liquid environment.

Modern scattering techniques have also been applied to the study of the structure of systems relevant in used nuclear fuel reprocessing. This has led to a deeper understanding of the formation of subphases in the extraction systems, especially the third phase formation in the organic phase.[1,2,6−8,13−16] Most recently, X-ray and neutron scattering experiments on a binary mixture of TBP/*n*-octane, have suggested the possibility of TBP dimer formation.[28]

In recent years, molecular modeling and simulation have been utilized to elucidate the fundamental molecular processes for some extraction systems. Wipff and co-workers have carried out molecular dynamics (MD) simulation of systems involving TBP, such as TBP in vacuum and in chloroform;[12] the stoichiometry of TBP complexation in aqueous solution,[29] and TBP complexation with uranyl nitrate and acid dissolution in supercritical CO_2.[30] We have also conducted a series of MD simulations with the aim of understanding uranyl complex formation in aqueous phase, its migration to the interface, and the effect of interface in facilitating the formation of various complex species, as well as the process of neutral species migration into the organic phase.[31−34]

Following an earlier work,[35] here we report on our studies of TBP/*n*-dodecane liquid mixture using all-atoms models aimed at testing the force-field models and the conventional standard combining rules. Specifically, we have computed various properties of the mixture in the liquid phase, namely: mass density, excess volume of mixing, the electric dipole moment variation with concentration, and the microscopic structure as characterized by the pair correlation functions and the arrangement of TBP molecules in the formation of TBP dimers. These computations have been carried out with two sets of molecular force fields. In the following, we will first describe the force field models and methods (see Section II). In turn, results are discussed in Section III, and a summary of our findings is provided in Section IV.

II. MODELS AND METHODS

For TBP, the Assisted Model Building with Energy Refinement intramolecular parameter set (AMBER99[36]) for bond length stretching, bond angle bending, and dihedral angle torsion[36−38] has been used. The total interaction potential energy is given below:

$$E = \sum_{\text{bonds}} K_r(r - r_{eq})^2 + \sum_{\text{angles}} K_\theta(\theta - \theta_{eq})^2 + \sum_{\text{dihedrals}} \left[\sum_n V_n(1 + \cos(n\phi - \gamma_n)\right] + \sum_{i<j} \left[\varepsilon_{ij}\left(\frac{R^*_{ij}}{r_{ij}}\right)^{12} - 2\varepsilon_{ij}\left(\frac{R^*_{ij}}{r_{ij}}\right)^{6} + \frac{q_i q_j}{r_{ij}}\right] \quad (1)$$

The terms in order of appearance in eq 1 are the bond length stretching, bond angle bending, bond torsion, van der Waals, and electrostatic interactions, respectively. The parameters for the interaction potential for TBP are given in Tables 1−4. For the van der Waals and electrostatic interaction between 1 and 4 atoms in the same TBP molecule, we have followed the AMBER convention, using the reduction parameters of 1/2 and 1/1.2, respectively.[35,38] A schematic molecular structure of the TBP molecule is shown in Figure 1 for reference.

Table 1. Bond Length Stretch Energy and Length Parameters for TBP Molecule in Eq 1

bond type	K_r [kcal/(mol Å^2)]	r_{eq} [Å]
OS−P	230	1.610
OS−CT	320	1.410
P−O2	525	1.480
CT−H	340	1.090
CT−CT	310	1.526

Table 2. Bond Angle Bending Energy and Angle Parameters for TBP Molecule in Eq 1

angle type	K_θ [kcal/(mol rad^2)]	θ_{eq} [deg]
CT−OS−P	100.0	120.5
OS−P−O2	100.0	108.23
OS−P−OS	45.0	102.6
OS−CT−H	50.0	109.5
OS−CT−CT	50.0	109.5
H−CT−H	35.0	109.5
CT−CT−H	50.0	109.5
CT−CT−CT	40.0	109.5

Table 3. Dihedral Torsion Energy and Angle Parameters for TBP Molecule in Eq 1

	V_n [kcal/mol], γ_n					
dihedral type	n = 1		n = 2		n = 3	
CT−OS−P−O2	0	0	0	0	0.25	0
CT−OS−P−OS	0	0	1.2	0	0.25	0
H−CT−OS−P	0	0	0	0	0.383	0
CT−CT−OS−P	0	0	0	0	0.383	0
OS−CT−CT−H	0.25	0	0	0	0.156	0
OS−CT−CT−CT	0	0	0	0	0.156	0
H−CT−CT−H	0	0	0	0	0.15	0
CT−CT−CT−H	0	0	0	0	0.16	0
CT−CT−CT−CT	0.2	180	0.25	180	0.18	0

The all-atom optimized potentials for liquid simulations (OPLS-AA) force field model was used for *n*-Dodecane.[39,40] The model uses the same form of potential as in eq 1, with only a slight change in the form of the torsion potential, which is given explicitly below as

dx.doi.org/10.1021/jp5040135 | J. Phys. Chem. B 2014, 118, 10750−10760

Table 4. Lennard-Jones and Electric Charge Parameters for TBP Molecule in Eq 1[a]

atom type	AMBER ε_i (kcal/mol)	AMBER σ_i (Å)	OPLS ε_i (kcal/mol)	OPLS σ_i (Å)	MNDO q_i (e)	DFT/RHF q_i (e)
O2	0.2100	2.960	0.2100	2.960	−0.522	−0.56581
P	0.2000	3.742	0.2000	3.742	1.062	1.12672
OS	0.1700	3.000	0.1700	3.000	−0.336	−0.43106
C0	0.1094	3.400	0.0660	3.500	0.120	0.25459
C1	0.1094	3.400	0.0660	3.500	0.036	0.01820
C2	0.1094	3.400	0.0660	3.500	0.012	0.08491
C3	0.1094	3.400	0.0660	3.500	0.012	−0.02282
H0	0.0157	2.650	0.0300	2.500	−0.012	−0.01827
H1	0.0157	2.650	0.0300	2.500	0.000	0.00049
H2	0.0157	2.650	0.0300	2.500	0.000	−0.02709
H3	0.0157	2.650	0.0300	2.500	0.000	−0.00035

[a]The van der Waals parameters in eq 1 are related to the commonly used Lennard-Jones parameters in the σ form by $\sigma_{ij} = R^*_{ij}/(2)^{1/6}$, while ε_{ij} remains the same. The following combining rules are used for cross interactions: $\varepsilon_{ij} = (\varepsilon_i\varepsilon_j)^{1/2}$, $\sigma_{ij} = 1/2(\sigma_i + \sigma_j)$. Nonbonded interaction potentials for intramolecular 1−4 atoms of TBP molecule are applied with scaling factors 1/2 and 1/1.2 for van der Waals and electrostatics, respectively.

$$E(\phi) = \frac{V_1}{2}[1 + \cos(\phi + \gamma_1)] + \frac{V_2}{2}[1 - \cos(2\phi + \gamma_2)] + \frac{V_3}{2}[1 + \cos(3\phi + \gamma_3)] \quad (2)$$

The original parameters for the torsional potential were first published in ref 39, and a slightly modified set of parameters were published later in ref 40. In this work, the newer parameters were used in eq 2 for the torsion potential.

The van der Waals interaction of the OPLS-AA model is given by

$$E_{ij} = 4\varepsilon_{ij}\left[\left(\frac{\sigma_{ij}}{r_{ij}}\right)^{12} - \left(\frac{\sigma_{ij}}{r_{ij}}\right)^{6}\right] \quad (3)$$

Note that the van der Waals force parameters in the Lennard-Jones (LJ) form used in the OPLS-AA model in eq 3 are related to those in the AMBER form by $\sigma_{ij} = R^*_{ij}/2^{1/6}$, $\varepsilon_{ij}|_{\text{OPLS-AA}} = \varepsilon_{ij}|_{\text{AMBER}}$. We have recently shown that the intramolecular scaling factor for the van der Waals and the electrostatic interaction can have a significant effect on the chain stiffness of the *n*-dodecane molecule, and that the original OPLS-AA scaling factor was too large for ambient condition simulations.[41] Thus, in this study we have used a scaling factor of 0.3 for *n*-dodecane. In calculating the cross chemical species interaction parameters, we have used the Lorentz−Berthelot combining rules (adopted by AMBER, i.e., geometric average for the energy parameter and arithmetic average for the distance parameter) for interaction between dissimilar atoms for all cross interactions whether in the same molecular compound or between different molecular compounds. This involves a slight modification of the original OPLS-AA combining rules (which uses geometric averages throughout), the effect of which on the properties studied in this work is insignificant.

The details of the force fields for the TBP molecule were given in a previous publication. In that work, four different force field models were tested.[35] Overall, the OPLS-MNDO and OPLS-DFT/RHF force field perform best. Here the acronym after the hyphen refers to the method used to calculate the atomic partial charges on the TBP molecule, with MNDO being the "modified neglect of differential overlap" semiempirical quantum chemistry method[42] and DFT/RHF referring to using the "density functional theory" for geometry optimization and subsequently "restricted Hartree-Fock theory" for the partial charge fitting.[43,44] In both methods, the charges were obtained through fitting to the electrostatic potential (ESP) or with the appropriate constraint (RESP).[45,46] Due to the large computational effort required for carrying out the present study, we have focused our efforts on two force field models for TBP, i.e., the OPLS-DFT/RHF and the OPLS-MNDO that performed best in our earlier study.[35] In our previous work,[35] we also found that the original ESP or RESP charges tend to overestimate the dipole moment of the TBP molecules in liquid environment. The likely cause for this overestimate is that the TBP molecule has a large number of possible conformations and the atomic partial charges were obtained based on only one conformation. We have thus used rescaled atomic charges so that they correctly reproduce the experimentally measured electric dipole moment of TBP. For convenience, the LJ parameters and the rescaled atomic charges are listed in Table 4 (these are the charges scaled with a factor 0.7 in the OPLS-DFT/RHF model, and charges scaled with 0.6 in the OPLS-MNDO model, cf. Table 5 of ref 35).

The long-range electrostatic interaction is treated via Ewald sums,[47,48] and the calculation of the pressure followed the method described by Alejandrea et al.[49] The details can be found in the Supporting Information for interested readers.

The simulations were carried out in NVT ensemble using 500 TBP molecules at 25 °C. For the LJ interaction, a cutoff distance of 15 Å was used and the potential shifted. The standard long-range correction to the pressure from the LJ interaction is included.[48] The equation of motion was integrated using the reversible multiple time step method with the Nosé thermostat.[50−52] A time step of 0.3 fs was used for the fast intramolecular motion, and a time step of 1.5 fs was used for the integration of the intermolecular motion. Initial configurations were created by putting all molecules on lattice points with zero size (zero LJ size parameter), which were then slowly increased to the full size (normal LJ size parameter). The systems were then equilibrated for at least 1 ns and the configurations saved. All simulations were started from such saved configurations. The system was then equilibrated for at least 45 ps using a velocity rescaling thermostat and another 45 ps or longer. The pressure variation with time indicated that at the end of the equilibration, the pressure had relaxed to its equilibrium value. The equilibrium pressure from MD runs was mostly obtained in the 1.5 to 2.3 ns time frame, with some calculations executed for as long as 4.0 ns.

dx.doi.org/10.1021/jp5040135 | J. Phys. Chem. B 2014, 118, 10750−10760

III. RESULTS AND DISCUSSION

III.1. Properties of *n*-Dodecane Liquid Using the OPLS-AA Potential. In a prior publication, we have reported the properties of pure TBP liquid at ambient conditions. Here we first describe the mass density prediction of pure *n*-dodecane at ambient condition from the OPLS-AA model. In Figure 2, we show the calculated pressure as a function of mass

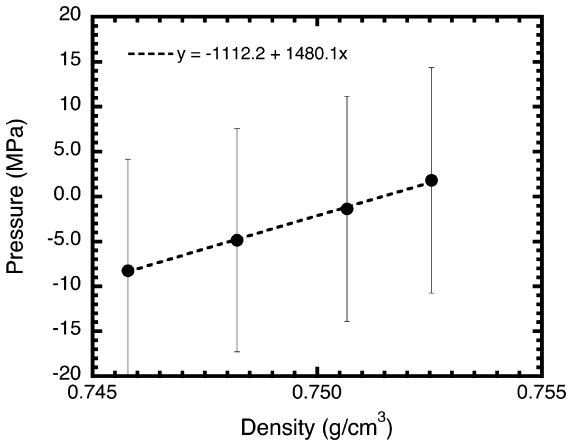

Figure 2. Calculated pressure versus density curve for *n*-dodecane. An interpolation of the linear fit to the data is used to obtain the density at ambient condition (T = 25 °C, P = 0.1 MPa).

density near the experimental mass density at ambient condition. Interpolation to ambient pressure (0.1 MPa) yields a mass density of 0.7514 g/cm^3. Compared to the experimental value of 0.7458 g/cm^3,[11] the model calculation predicts the mass density to within 99.3% accuracy. This close agreement establishes a basis for the mixture calculation.

III.2. Concentration Dependence of the TBP Electric Dipole Moment of the TBP/*n*-Dodecane Mixture. The average electric dipole moment for TBP, p_D, in liquid state was computed using NVT molecular dynamics which was obtained from eqs 4 and 5,

$$\mathbf{p}_m = \sum_j q_j(\mathbf{r}_{mj} - \mathbf{r}_m^{com}) \quad (4)$$

$$p_D = \left\langle \left(\frac{1}{N} \sum_{m=1}^{N} p_m^2 \right)^{1/2} \right\rangle \quad (5)$$

where $\mathbf{p}_m$ is the instantaneous dipole moment vector of a molecule, m. The summation in eq 4 runs through all atom j in a molecule. Equation 5 gives the ensemble average of the magnitude of the dipole moment over all TBP molecules in the system.

In Figure 3, we plot the variation of the TBP dipole moment as a function of the TBP molar fraction in the mixture. In the figure, the dipole moment for each concentration was obtained from averaging over the three densities near the ambient condition (cf. Supporting Information, Figures SI.1 and SI.2). As the difference between the three densities used for interpolating to the ambient density is small, they all give essentially the same dipole moment, and a simple averaging was used to obtain the dipole moment at the ambient condition. As can be seen from the figure, the dipole moment of TBP monotonically increases with the concentration of the TBP in

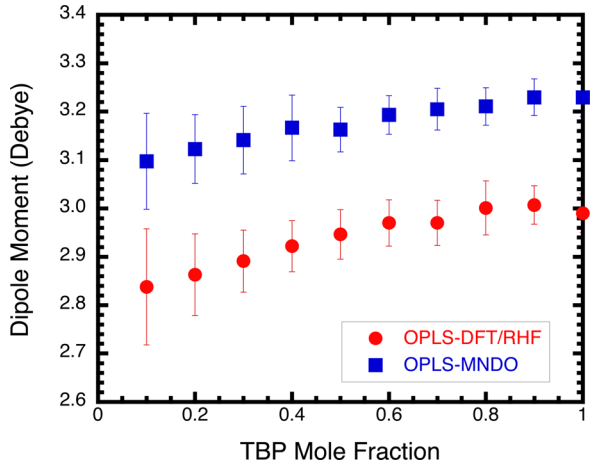

Figure 3. Dipole moment of TBP as a function of mole fraction. Circle and square symbols are for the DFT/RHF and MNDO charge model, respectively.

the mixture. The magnitude of the variation over the whole concentration range, however, is not large, from 2.84 to 2.99 D, or about 5.3% for the DFT/RHF-charge model, and from 3.10 to 3.23 D, or about 4.2% for MNDO-charge model, respectively. There are to date no reported experimental data on the TBP dipole moment in *n*-dodecane. However, some insight can be gained from other diluents. In dilute hexane, for example, experiment gives a value of 2.92 D;[53] in dilute cyclohexane, 2.76 D;[53] in *n*-octane, 2.6 D.[54] For pure TBP, experimental values of 3.07 and 3.32 D have been reported.[53,54] Hence it is reasonable to assume that TBP molecules behave similarly in *n*-dodecane as in other *n*-alkane diluents. Thus, the calculated variation of the TBP dipole moment is consistent with experimentally measured values, and it reasonably captures the trend of the dipole moment increase with concentration. These data also suggest that the dipole moment of TBP molecules in *n*-alkane solvent is not strongly affected by the variation in TBP concentration. Physically, this can be attributed to two factors. First, the fact that the *n*-alkanes are electrically neutral and apolar molecules hence their presence as a solvent does not significantly alter the polarity of the TBP. The other factor is that the TBP molecule, although polar, has a relatively small polarity when taking into consideration its molecular size as compared to water, for example. This is reflected in the low dielectric permittivity of pure TBP, with a dielectric constant of 8.14;[53] note that water has a dielectric constant of 78.5 at 25 °C.[55] It should be noted that the good agreement was anticipated since the partial charge for pure TBP was rescaled to reproduce its dipole moment. The interesting result is the mole fraction dependence of the dipole moment.

III.3. Mass Density of the TBP/*n*-Dodecane Mixture. Constant NVT simulations were performed at T = 25 °C for three densities near the experimentally measured density of the TBP/*n*-dodecane mixture at ambient conditions.[11] The calculated pressures for each mole fraction are plotted against density (Supporting Information, Figures SI.1 and SI.2) for the two force field models: OPLS-DFT/RHF and OPLS-MNDO, respectively. The mass density for the mixture was then obtained from interpolation to the pressure equal to 1 bar. The resulting mass density of the mixture is shown in Figure 4, along with the experimental data. The mass densities of pure TBP for the two models are taken from our previously published work.[35] The error bars appear large; the reason is

dx.doi.org/10.1021/jp5040135 | J. Phys. Chem. B 2014, 118, 10750−10760

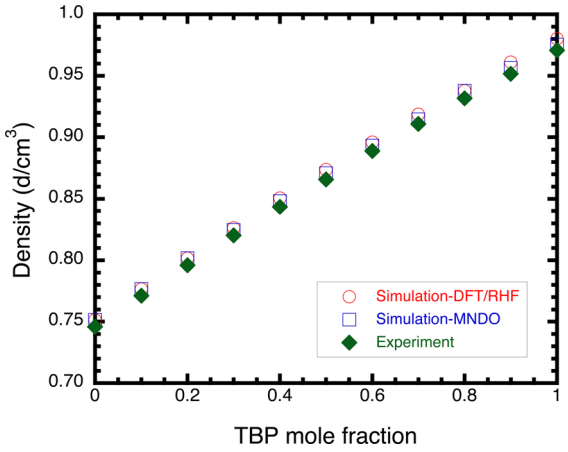

Figure 4. Mass density of the TBP/n-dodecane mixture as a function of the mole fraction. Open circles and squares are for the DFT/RHF and MNDO charge, respectively. Solid diamonds are from experiment.

that we have chosen to focus our effort near the atmospheric pressure and varied density by a very small amount, 0.5%. If we had varied the density to cover a larger span, the error bar would have been relatively small. Nevertheless, the monotonic variation of the average pressure with the density suggests the average pressure values obtained are reliable.

It is seen that over the entire range of TBP mole fraction 0 to 1, the two force field models accurately reproduce the experimentally measured mass density. Although the calculations predict a slightly higher mixture density, the maximum deviation from the experimental value is about 1.0% for the OPLS-DFT/RHF model, which occurs at high TBP concentration, and 0.76% for the OPLS-MNDO model, which occurs at low TBP concentration. Thus, by simply applying the commonly used Berthelot-Lorentz combining rules for the interaction parameters between the two model types of molecules, TBP and *n*-dodecane, highly accurate mass density at ambient condition is obtained for the mixture.

III.4. Excess Volume of Mixing. The excess volume of mixing is a quantity of great interest, partly because it can be easily measured in experiment. At the molecular level, the volume of mixing is a result of complex combination of molecular properties between two molecular species such as size, shape, as well as the inherent molecular interaction. Experiments have found that the excess volume of mixing between TBP and *n*-alkanes is dependent on the chain length. For short *n*-alkanes, such as *n*-hexane, the excess volume is negative,[11] very likely a result of the relatively small difference between the *n*-hexane and the *n*-butyl tails of the TBP, which make them more compatible in spatial packing. For *n*-dodecane, the experimentally measured excess volume is positive, a result of the disparate shape of the two types of molecule and the fact that the *n*-dodecane chain is much longer than the *n*-butyl tails of the TBP molecule. The magnitude of the excess volume, however, is relatively small, less than 0.9 cm^3/mol compared to the molar volume of 228.4 cm^3/mol for *n*-dodecane and 274.4 cm^3/mol for TBP based on experimental data.[11] Thus, the prediction of the excess molar volume provides a much more stringent test of the force field models.

We have calculated the excess molar volume, ΔV_{ex}, by subtracting the pure component molar volume from the mixture molar volume, using the following equation:[11]

$$\Delta V_{ex} = \frac{x_1M_1 + x_2M_2}{\rho} - \frac{x_1M_1}{\rho_1} - \frac{x_2M_2}{\rho_2} \quad (6)$$

where x_1 and x_2 are mole fractions, M_1 and M_2 are the molar masses, and ρ_1 and ρ_2 are the densities of pure components 1 (TBP) and 2 (*n*-dodecane), respectively; ρ is the density of the mixture.

Figure 5a,b displays the excess volume calculated using the two force field models, OPLS-DFT/RHF and OPLS-MNDO,

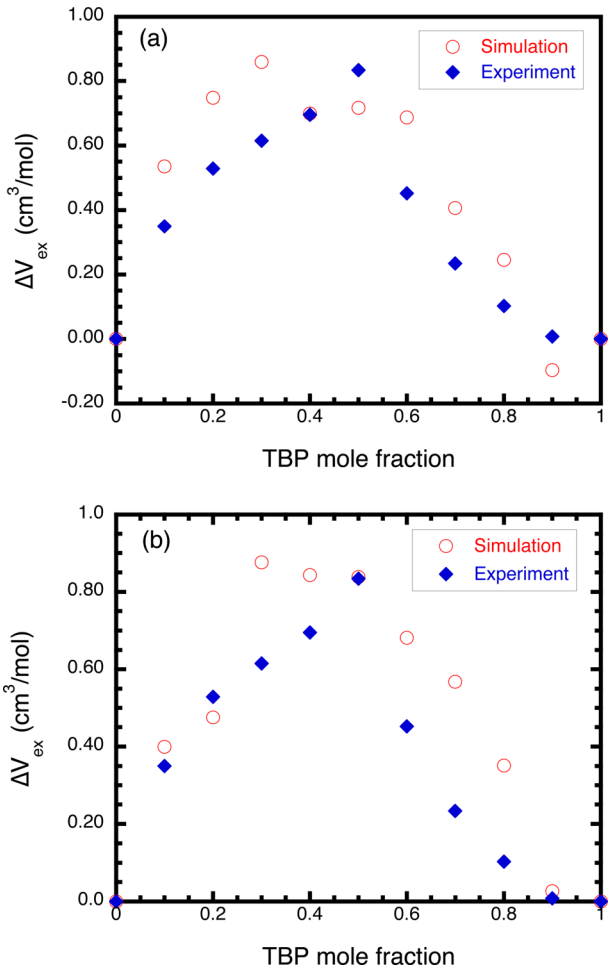

Figure 5. Excess volume of mixing for the TBP/*n*-dodecane mixture as a function of the TBP mole fraction. (a) DFT/RHF-charge model. (b) MNDO charge model. Open circles are from simulation, and the solid diamonds are from experiment.

respectively. It is seen that both models correctly predict the increase of the molar volume upon mixing, as obtained experimentally. In general, the model calculations also reasonably predict the trend of the variation of the excess volume with the mole fraction, i.e., the rapid initial rise at small TBP mole fraction, with a maximum excess volume in the mid region of mole fraction, and relatively small excess volume at high TBP concentration. This trend can be rationalized as follows.

Within statistical uncertainty, the calculated excess volume peaks between 0.3 and 0.5 mole fraction, consistent with the experimentally measured excess volume, which peaks at around mole fraction of 0.5. The initial rapid rise is probably a result of the strong disruptive effect of the TBP molecules in an *n*-dodecane liquid because of their disparate molecular shape

dx.doi.org/10.1021/jp5040135 | J. Phys. Chem. B 2014, 118, 10750−10760

(TBP is more or less globular, whereas the *n*-dodecane is linear). At high TBP concentration, the effect of the *n*-dodecane molecules in a TBP dominated liquid is substantially reduced because of the strong interaction between the TBP molecules. The excess volume is a much smaller quantity than the molar volume, less than 1% in comparison. Therefore, even when the density (equivalently the molar volume) is well reproduced by the model, the excess volume may not be reproduced with the same level of accuracy. In fact, we consider obtaining the correct sign for the excess volume, a good indicator for accuracy of the simulations.

III.5. Self-Diffusion of TBP and *n*-Dodecane in the Mixture. The self-diffusion coefficients for the two components in the mixture were calculated starting from the previously equilibrated configurations at a few prototypical mole fractions: 30, 50, and 80% for the OPLS-/RHF model, and at 50% mole fraction for the OPLS-MNDO model. The center-of-mass of each molecule was collected every15 fs and in total a 1.5 ns calculation was performed for each mole fraction and a trajectory of 0.75 ns was used for averaging the center of mass data. The mean-square-displacements (MSDs) are displayed in Figure 6 and the linear fit was used to obtain the self-diffusion coefficient. For OPLS-DFT/RHF model, we obtain the diffusion coefficient for TBP: $(1.460 \pm 0.131) \times 10^{-6}$, $(1.135 \pm 0.208) \times 10^{-6}$, $(0.563 \pm 0.076) \times 10^{-6}$ cm^2/s, at the three mole fractions, 30%, 50%, and 80%, respectively; for *n*-dodecane: $(3.224 \pm 0.332) \times 10^{-6}$, $(2.321 \pm 0.0.105) \times 10^{-6}$, $(1.252 \pm 0.0.365) \times 10^{-6}$ cm^2/s at the three mole fractions, respectively. For the OPLS-MNDO model, we calculated the diffusion coefficients at mole fraction 50% for comparison between the two models. The self-diffusion coefficients obtained are $(1.294 \pm 0.118) \times 10^{-6}$ cm^2/s for TBP and $(2.451 \pm 0.093) \times 10^{-6}$ cm^2/s for *n*-dodecane, respectively. These values of the self-diffusion coefficient show a decreasing trend with increased mole fraction of TBP. This is understandable, as pure TBP liquid has an experimental self-diffusion coefficient of 2.29×10^{-6} cm^2/s and *n*-dodecane liquid has an experimental self-diffusion coefficient of 8.71×10^{-6} cm^2/s. For the model prediction, the OPLS-DFT/RHF gives a value of $(0.499 \pm 0.59) \times 10^{-6}$ cm^2/s and OPLS-MNDO gives a value of $(0.509 \pm 0.24) \times 10^{-6}$ cm^2/s for pure TBP;[34] while model prediction for *n*-dodecane gives a value of $(4.883 \pm 0.208) \times 10^{-6}$ cm^2/s.[41] Thus, the mole fraction dependence of the self-diffusion observed for the mixture is entirely consistent with the pure substances. It is noted that, to our best knowledge, there are no experimental data available for the self-diffusion coefficient in the mixture studied here. Based on the comparison for pure substances, the predicted self-diffusion for TBP in the mixture is likely low, and similarly for *n*-dodecane.

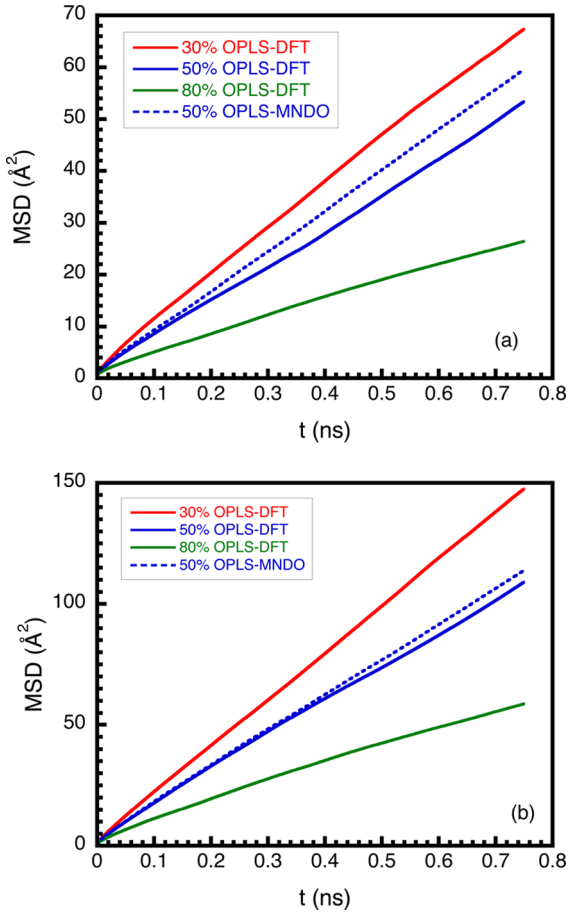

Figure 6. Mean square displacement (MSD) for TBP and *n*-dodecane in the mixture: (a) MSD for TBP; (b) MSD for *n*-dodecane.

III.6. Spatial Pair Correlation Functions (PCFs) and Self-Association of TBP. The spatial PCFs between atoms of two interacting molecules can be used to gain insight into the microstructure of TBP in the liquid state. Such structural information can also be derived based on X-ray and/or neutron scattering measured structure factor. An analysis of the PCFs is also useful from a theoretical perspective in providing insight into macroscopic properties of the system as well as how molecules interact in the liquid state bulk phase. Based on a host of experimental techniques, namely, distribution coefficient experiments,[18] infrared spectroscopy,[19] nuclear magnetic resonance,[20] calorimetry,[21−25] and vapor pressure osmometry,[26,27] it has been suggested that TBP in liquid environment has a tendency for self-association. More recently, Motokawa et al. have carried out X-ray and neutron scattering experiments on TBP/*n*-octane mixture,[28] and reported observing a peak in X-ray scattering intensity at wave vector $q \approx 0.63-0.68$ (corresponding to a wavelength of $\lambda = 2\pi/q \approx 0.94-0.98$ nm) which the authors attributed to the average P−P distance in the mixture.

In a prior publication, we reported on the PCFs for pure TBP liquid.[35] Here we report on the PCFs for the TBP/*n*-dodecane liquid, and discuss the effect of concentration variation. We also analyze the probable arrangement between two interacting TBP molecules in the solution, and in the process comment on the evidence for self-association (or dimerization). It is noted that the strongest interaction between TBP molecules occurs through the atoms on the phosphoryl headgroup, mainly involving the P and the O2 atoms (cf. Figure 1). Physical consideration suggests a dimerization through the electrostatic attraction of the TBP dipoles. To determine the relative position between two interacting TBP molecules and their orientational arrangement, the PCFs for P−P, P−O2, and O2−O2, are analyzed. In the following, we will first present the PCFs involving P and O2 atoms on the TBP head groups that are more relevant to the self-association of TBP. The rest of the PCFs are shown in the Support Information.

(a). P−P Pair Correlation Function. Figure 7a,b shows PCFs for P−P using the DFT/RHF and MNDO charge models, respectively, for TBP concentration of 10%, 50%, 90% mole

dx.doi.org/10.1021/jp5040135 | J. Phys. Chem. B 2014, 118, 10750−10760

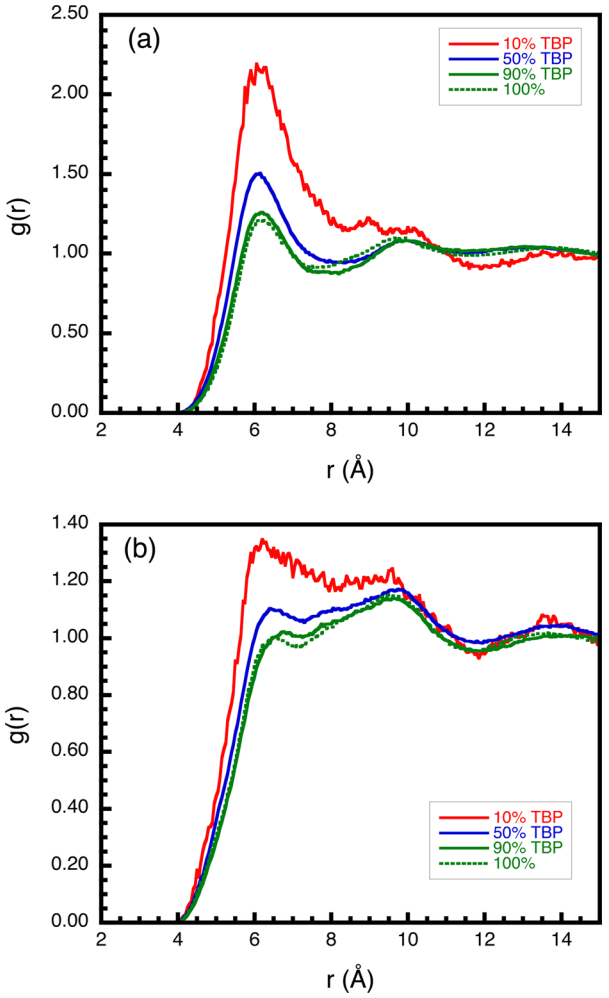

Figure 7. Spatial PCF between the P atoms of two TBP molecules at selected TBP concentrations: (a) DFT/RHF-charge model. (b) MNDO-charge model. The red, blue, and green solid curves are for 10%, 50%, and 90% TBP mole fraction, respectively. The dotted curve is for pure TBP.

fraction, and pure TBP. Although the details in terms of the peak height are somewhat different for the two charge models, both give the locations of the peak height at about the same distances: a first P−P peak at approximately around 6.1−6.5 Å, and a second P−P peak around 9.8 Å.

The locations of the peaks in the PCFs should correspond to the locations of peaks in the measured structure factor in scattering experiments, usually expressed in terms of wave vector, q. The first peak position at ∼6.1 Å in the PCF corresponds to a wave vector $q \approx 2\pi/\lambda \approx 10.3$ nm^{-1}. The second peak position at 0.98 nm (corresponding to a wave vector q of 6.4 nm^{-1}) in the P−P PCF is consistent with the experimentally measured X-ray scattering intensity peak location, if the location of the scattering intensity location can be identified with the location of the structure factor. In addition, the experimentally observed mole fraction dependence of $I(q = 0)$ (ref 28, Figure 5b,c) can be qualitatively explained from the strong interaction between TBP molecules (based on fluctuation theory of scattering (ref 28, eq 2).

We note that in Figure 7b, the second peak is higher than the first peak for mole fraction higher than 50%. This likely suggests an exclusion effect for the first nearest neighbors. Interestingly, the second peak occurs at a distance close to scattering experiment measured dimer distance. Further studies are required to identify the precise structure leading to this peak.

(b). P−O2 Pair Correlation Function. The P−O2 PCFs for two TBP molecules are displayed in Figure 8a,b. Again, the

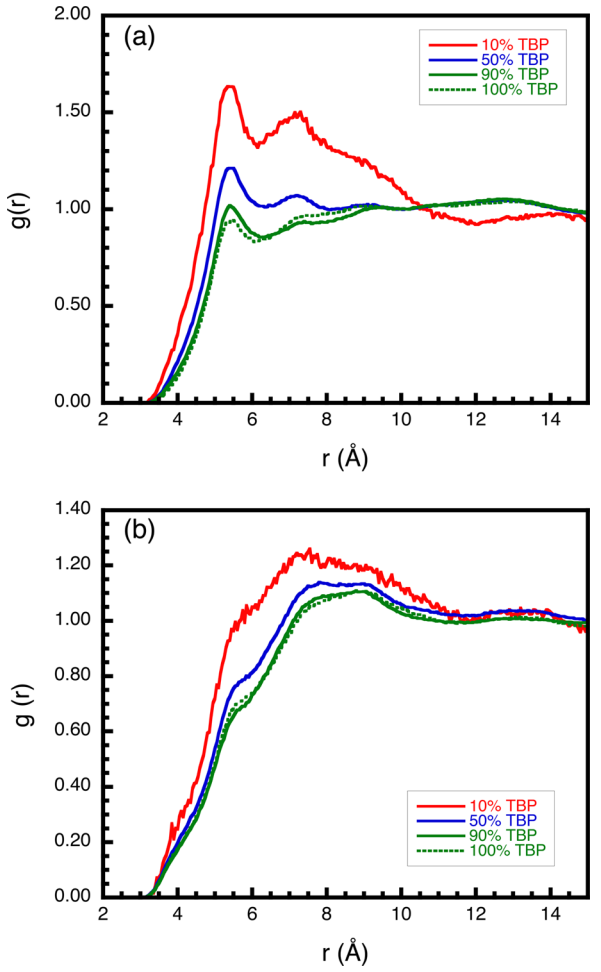

Figure 8. Spatial pair correlation function between the P and O2 atoms of two TBP molecules at selected TBP concentrations. (a) DFT/RHF-charge model. (b) MNDO-charge model. The red, blue, and green solid curves are for 10%, 50%, and 90% TBP mole fraction, respectively. The dotted curve is for pure TBP.

same essential features are exhibited in the PCFs from the two different charge models. For the DFT/RHF-charge model, the first peak occurs at around 5.4 Å; while for the MNDO-charge model, this peak appears as a shoulder. The second peak for DFT/RHF occurs at around 7.2 Å, while for MNDO model it is broadened and occurs around between 7.2−7.7 Å, depending on the concentration, and showing signs of overlap with a third peak at larger distance beyond 7.7 Å.

(c). O2−O2 Pair Correlation Function. Figure 9a,b shows the PCFs between the O2 atom of two TBP molecules. For DFT/RHF-charge model, a shoulder appears at about 5.2 Å and a peak appears at about 6.6 Å. For the MNDO-charge model, similar essential features are observed, although less prominent than for the DFT/RHF charge model with a slight shift to larger distances for the shoulder and the peak. The shoulder is less obvious at high concentration but is clearly visible for 10% TBP concentration, at about 5.3 Å. The peak appears between 7.0 and 7.6 Å depending on the concentration.

dx.doi.org/10.1021/jp5040135 | J. Phys. Chem. B 2014, 118, 10750−10760

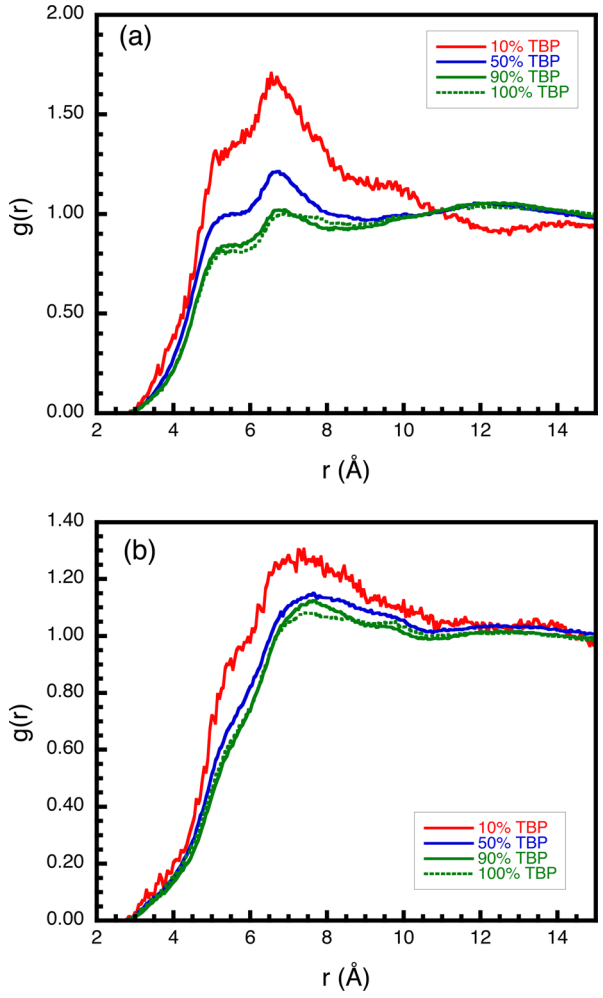

Figure 9. Spatial pair correlation function between the O2 atoms of two TBP molecules at selective TBP concentration for DFT/RHF charge model (a), and MNDO charge model (b). The red, blue, and green solid curves are for 10%, 50%, and 90% TBP mole fraction, respectively. The dotted curve is for pure TBP.

The first peak in PCF is determined by the van der Waals exclusion at short distance and the mean attraction between the atom pairs in the liquid environment. The lack of structure in PCF for the OPLS-MNDO model in comparison with the OPLS-DFT/RHF model is likely due to the fact that the OPLS-DFT/RHF charge is slightly larger and it exhibits more variations in partial atomic charges from site to site (cf. Table 4). It should also be noted that in this system that the electrostatic interaction is much stronger than van der Waals interaction.

With the knowledge of the P−P, P−O2, and O2−O2 pair correlation functions, one can deduce the most likely molecular arrangement between the two TBP molecules, specifically, the relative orientation of the head groups of the two TBP molecules, to shed light on the self-association of TBP that has been suggested based on experimental evidence.[1] We assume here an arrangement of close encounter between two TBP molecules, for which the interaction is the strongest. This corresponds to the first peak position (or shoulder) of the PCFs for P−P, P−O2, and O2−O2.

For illustration, we used values in the PCF for the DFT/RHF-charge model. Because of the similarity in the essential features of the two sets of PCFs, the analysis applies to both charge models. We start by utilizing the P−P PCF wherein the first peak position is at 6.10 Å.

With the P−P distance fixed at 6.10 Å, we can arrange the relative position of the O2 atoms by rotating P−O2 bond around P, keeping in mind that the P═O2 bond distance is 1.48 Å. This means that the allowable position for each O2 is on a spherical surface around the P atom of each TBP molecule. For ease of understanding, we first discuss a few simple arrangements, which are illustrated in Figure 10.

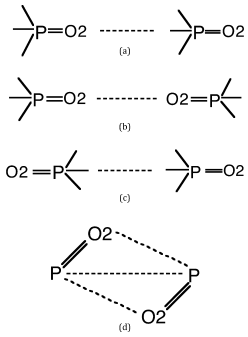

Figure 10. Possible arrangements of the headgroup of two TBP molecules at close contact. The three tail groups are represented with straight lines for simplicity. (a) The head dipoles are aligned on a line with the same orientation. (b) The head dipoles are aligned on a line in opposite orientation with dipoles pointing outward. (c) The head dipoles are aligned on a line in opposite orientation with dipoles pointing inward. (d) The head dipoles form an antiparallel dimer configuration which provides a most favorable electrostatic interaction between the two dipoles.

(1) The two P═O2 bonds are aligned on a line in the same orientation (Figure 10a), and we can deduce that there are two possible distances between P and O2 atoms from two TBP molecules: d_{P-O2} = 6.10 + 1.48 = 7.58 Å, and d_{P-O2} = 6.10−1.48 = 4.62 Å, respectively. The P═O2 PCF suggests that this arrangement is not realized, as there are no peaks appearing at these positions.

(2) The two P═O2 bonds are aligned on a line in opposite orientation, with the two O2 atoms inside (Figure 10b). The distance between P and O2 atoms is d_{P-O2} = 6.10−1.48 = 4.62 Å. As in case (1), there exists no peak at this position in the PCF either.

(3) The two P═O2 bonds are aligned on a line in opposite orientation, with the two O2 atoms outside (Figure 10c). The distance between P and O2 atoms is, d_{P-O2} = 6.10 + 1.48 = 7.58 Å. Similarly, no peak exists in the PCF at this position.

(4) The two P═O2 bonds are in the same plane, the case of a parallelogram (Figure 10d). From the P−O2 PCF, we see that the actual peak occurs around 5.40 Å, which is between the two extreme cases of (2) and (3), closer to case (2) than case (3). This suggests that the actual orientation can be obtained by starting from case (2) and rotate both bonds an angle θ (θ < 90°) in opposite direction, as shown in Figure 10d. Using

$$d_{O2-O2}^2 = d_{P-O2}^2 + b_{P=O2}^2 - 2d_{P-O2}b_{P=O2}\cos\phi$$

with d_{O2-O2} = 5.2 Å (first shoulder position in O2−O2 PCF), d_{P-O2} = 5.40 Å, and $b_{P=O2}$ = 1.48 Å, we obtain ϕ = ∠O2PO2 = 74.4°. Since the ∠O2PO2 angle is less than 90°, the arrangement in Figure 10d provides

dx.doi.org/10.1021/jp5040135 | J. Phys. Chem. B 2014, 118, 10750−10760

favorable electrostatic interaction between two TBP molecules with the two TBP dipoles in antiparallel alignment with the positively charged P and the negatively charged O2 closest to each other. Thus, the geometry from MD simulation provides an explicit realization for the TBP molecule dimerization conjectured from a variety of experimental evidence.[18−28]

The above analysis gives rough guidance on the possible orientation of two TBP molecules in a dimer configuration. To more quantitatively analyze the TBP dimer formation, we computed the angular distribution function at a range of fixed distances between 4.0 and 7.0 Å. These are displayed in Figure 11 and Figure SI. 10. In the figure, all the contribution from P−P distance less than 4.0 Å are collected into the 4.0 Å bin, each subsequent distance represent the contribution for distances between the labeled distance and the immediate smaller one, with a resolution of 0.5 Å. Specifically, the angular dependent distribution function for mole fractions 30% and 50% for both the OPLS-DFT/RHF and OPLS-MNDO models are displayed. For the OPLS-DFT/RHF model, the angular distribution shows a clear peak at about 140 degrees at distances between 5.0 and 6.0 Å (see Figure 11). This suggests less than the perfect alignment of two TBP with the two dipoles in antiparallel configuration, as this configuration would correspond to an angle of 180°. Evidently, there are significant population of molecules at other angles less than 140°. This is due to the fact that the radial distribution functions (cf. Figures 7−9) are not very pronounced, which leads to a relatively diffuse angular distribution.

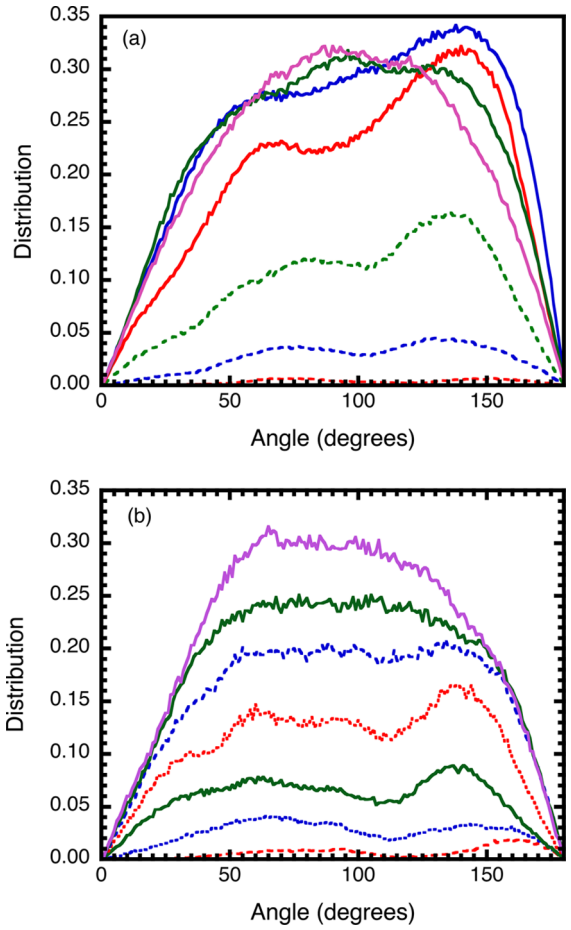

Figure 11. Distribution as a function of angle of the P═O bonds between two TBP molecules at various distances from 4.0 to 7.0 Å: dashed red line (4.0 Å), dashed blue line (4.5 Å), dashed green line (5.0 Å), solid red line (5.5 Å), solid blue line (6.0 Å), solid green line (6.5 Å), solid purple line (7.0 Å). (a) OPLS-DFT/RHF model at 30% mole fraction. (b) OPLS-MNDO model at 30% mole fraction.

This can also be seen from the angular distributions for the OPLS-MNDO model, where the radial distribution function is less pronounced than for the OPLS-DFT/RHF model, which shows a relatively lower peak at about 140° in comparison. This can be compared to the angular distribution at larger distances, where it is seen for both models that the peak occurs at around 90°.

IV. CONCLUSIONS

The performance of two sets of force field models for TBP in predicting the TBP/*n*-dodecane mixture thermophysical properties in the liquid state has been examined. The results show that both the OPLS-DFT/RHF and OPLS-MNDO models accurately predict the mass density, to better than ∼1.0%. Both models correctly predict the trend of the variation of the TBP dipole moment with the TBP concentration in the *n*-dodecane diluent, and an increase of volume of mixing over the entire range of the mole fraction. The predicted excess volume of mixing suggests a maximum between 0.3 to 0.5 TBP mole fraction; which is reasonably consistent with experimental data within statistical uncertainty, where the excess volume of mixing is largest around 0.5 mole fraction.

We have calculated a variety of pair correlation functions (PCFs) for the TBP/*n*-dodecane mixture. Utilizing the PCFs for P−P, P−O2, and O2−O2 atom pairs between two TBP molecules, we carried out an analysis of possible relative arrangement of two TBP phosphoryl head groups in close contact. The results suggest a most probable dimer configuration with the two P═O2 bonds antiparallel to each other. This arrangement minimizes the interaction energy between two dipoles and is consistent with fundamental physics considerations and thus provide a reasonable explanation to a variety of experimental observations on dimer formation.

■ ASSOCIATED CONTENT

Supporting Information

Additional pair correlation functions for atom pairs other than those reported in the main text are available in the Supporting Information. This material is available free of charge via the Internet at http://pubs.acs.org/.

■ AUTHOR INFORMATION

Corresponding Authors

*E-mail: scui@utk.edu.
*E-mail: bkhomami@utk.edu.

Notes

The authors declare no competing financial interest.

■ ACKNOWLEDGMENTS

This work was supported by the U.S. Department of Energy, Office of Nuclear Energy under the Nuclear Energy University Program (DOE-NEUP), contract number: DE-AC07-051D14517. Computing resources used at the Center for Advanced Modeling and Simulation at the Idaho National Laboratory through a collaboration with the Nuclear Energy Advanced Modeling and Simulation program of the Nuclear

Energy Office of DOE are greatly appreciated. The Oak Ridge National Laboratory is managed by UT-Battelle, LLC for the DOE under contract No. DE-AC05-00OR22725.

REFERENCES

(1) Schultz, W. W.; Navratil, J. S.; Eds.; *The Science and Technology of Tributyl Phosphate*; CRC Press: Boca Raton, FL, 1984; Vol. *1*.
(2) Moyer, B. A., Ed. Solvent Extraction: Fundamentals to Industrial Applications. In *Proceedings of ISEC 2008 Conference*; Canadian Institute of Mining, Metallurgy and Petroleum: West Montreal, Quebec, Canada, 2008.
(3) Chiarizia, R.; Jensen, M. P.; Borkowski, M.; Ferraro, J. R.; Thiyagarajan, P.; Littrell, K. C. Third Phase Formation Revisited: The U(VI), HNO_3–TBP, *n*-dodecane System. *Solvent Extr. Ion Exch.* **2003**, *21*, 1–27.
(4) Chiarizia, R.; Nash, K. L.; Jensen, M. P.; Thiyagarajan, P.; Littrell, K. C. Application of the Baxter Model for Hard Spheres with Surface Adhesion to SANS Data for the U(VI)–HNO_3, TBP–*n*-Dodecane System. *Langmuir* **2003**, *19*, 9592–9599.
(5) Zilberman, B. Ya.; Fedorov, Yu. S.; Kopyrin, A. A.; Arkhipov, S. A.; I. V. Blazheva, I. V.; Glekov, R. G. Extraction of U(IV) and U(VI) with 30% Tributyl Phosphate under Conditions of Formation of the Second Organic Phase. *Radiochemistry* **2001**, *43*, 172–176.
(6) Shukla, J. P.; Misra, S. K. Carrier-Facilitated Transport of Plutonium(IV) through Tributyl Phosphate/Dodecane Liquid Membranes. *Indian J. Chem., Sect. A: Inorg., Bio-inorg., Phys., Theor. Anal. Chem.* **1995**, *34*, 778–786.
(7) Plaue, J.; Gelis, A.; Czerwinski, K.; Thiyagarajan, P.; Chiarizia, R. Small-Angle Neutron Scattering Study of Plutonium Third Phase Formation in 30% TBP/HNO_3/Alkane Diluent Systems. *Solvent Extr. Ion Exch.* **2006**, *24*, 283–298.
(8) Chiarizia, R.; Jensen, M. P.; Rickert, P. G.; Kolarik, Z.; Borkowski, M.; Thiyagarajan, P. Extraction of Zirconium Nitrate by TBP in *n*-Octane: Influence of Cation Type on Third Phase Formation According to the "Sticky Spheres" Model. *Langmuir* **2004**, *20*, 10798–10808.
(9) Nave, S.; Mandin, C.; Martinet, L.; Berthon, L.; Testard, F.; Madicc, C.; Zemb, Th. Supramolecular Organisation of Tri-*n*-butyl Phosphate in Organic Diluent on Approaching Third Phase Transition. *Phys. Chem. Chem. Phys.* **2004**, *6*, 799–808.
(10) Wright, A.; Paviet-Hartmann, P. Review of Physical and Chemical Properties of Tributyl Phosphate/Diluent/Nitric Acid Systems. *Sep. Sci. Technol.* **2010**, *45*, 1753–1762.
(11) Tian, Q.; Liu, H. Densities and Viscosities of Binary Mixtures of Tributyl Phosphate with Hexane and Dodecane from (298.15 to 328.15) K. *J. Chem. Eng. Data* **2007**, *52*, 892–897.
(12) Beudaert, P.; Lamare, V.; Dozol, J. F.; Troxler, L.; Wipff, G. Theoretical Studies on Tri-*n*-butyl Phosphate: MD Simulations in Vacuo, in Water, in Chloroform, and at a Water/Chloroform Interface. *Solvent. Extr. Ion Exch.* **1998**, *16*, 597–618.
(13) Chiarizia, R.; Rickert, P. G.; Stepinski, D.; Thiyagarajan, P.; Littrell, K. C. SANS Study of Third Phase Formation in the HCl–TBP–*n*-Octane System. *Solvent Extr. Ion Exch.* **2006**, *24*, 125–148.
(14) Chiarizia, R.; Briand, A.; Jensen, M. P.; Thiyagarajan, P. SANS Study of Reverse Micelles Formed upon the Extraction of Inorganic Acids by TBP in *n*-Octane. *Solvent Extr. Ion Exch.* **2008**, *26*, 333–359.
(15) Chiarizia, C.; Stepinski, D.; Antonio, M. R. SANS Study of HCl Extraction by Selected Neutral Organophosphorus Compounds in *n*-Octane. *Sep. Sci. Technol.* **2010**, *45*, 1668–1678.
(16) Antonio, M. R.; Chiarizia, R.; Jaffrennou, F. Third-Phase Formation in the Extraction of Phosphotungstic Acid by TBP in *n*-Octane. *Sep. Sci. Technol.* **2010**, *45*, 1689–1698.
(17) Osseo-Asare, K. Aggregation, Reversed Micelles, and Microemulsions in Liquid–Liquid Extraction: The Tri-*n*-butyl Phosphate–Diluent–Water–Electrolyte System. *Adv. Colloid Interface Sci.* **1991**, *37*, 123–173.
(18) Dyrssen, D.; Petkovic, D. M. Distribution Studies of Tripropyl Phosphate between Different Organic Diluents and Water. *J. Inorg. Nucl. Chem.* **1965**, *27*, 1381–1393.
(19) Petkovic, D. M. Some Correlations of Trialkyl Phosphates Dimerization Constants. *J. Inorg. Nucl. Chem.* **1968**, *30*, 603–609.
(20) Petkovic, D. M.; Kezele, B. A.; Rajic, D. R. Dipole Moments of Some Neutral Organic Phosphates. *J. Phys. Chem.* **1973**, *77*, 922–924.
(21) Afanasev, Y. A.; Nikolaev, A. V.; Koroleva, T. I. Thermochemistry of Binary Systems: I. TBP–Diluent Systems. *Soviet Radiochem.* **1966**, *8*, 634–636.
(22) Tsimering, L.; Kertes, A. S. Excess Enthalpies of Tri-*n*-butylphosphate + Hydrocarbons. *J. Chem. Thermodyn.* **1974**, *6*, 411–415.
(23) Tsimering, L.; Kertes, A. S. Correlation of Excess Enthalpies of Mixing in Tributylphosphate-*N*-Alkane System. *Thermochim. Acta* **1975**, *12*, 206–208.
(24) Tsimering, L.; Kertes, A. S. Enthalpies of Mixing of Tributylphosphate with Hydrogen-Bonding Solvents. *J. Chem. Eng. Data* **1977**, *22*, 163–165.
(25) Rytting, J. H.; Goldkamp, A.; Lindenbaum, S. Heats of Dilution of Trialkyl Phosphates in Iso-Octane and Carbon-Tetrachloride – Interpretations in Terms of Self-Association. *J. Solution Chem.* **1975**, *4*, 1005–1010.
(26) Rozen, A. M.; Khorkhorina, L. P.; Yurkin, V. G.; Novikova, N. M. Interaction of Tributyl Phosphate and Tributyl Phosphate Solvate with Diluents. *Dokl. Akad. Nauk SSSR* **1963**, *153*, 1387–1390.
(27) Poczynailo, A.; Danesi, P. R.; Scibona, G. Solvation of Uranyl Nitrate by TBP in *n*-Hexane by Vapor-Pressure Lowering Measurement. *J. Inorg. Nucl. Chem.* **1973**, *35*, 3249–3255.
(28) Motokawa, R.; Suzuki, S.; Ogawa, H.; Mark, R.; Antonio, M. R.; Yaita, T. Microscopic Structures of Tri-*n*-butyl Phosphate/*n*-Octane Mixtures by X-ray and Neutron Scattering in a Wide *q* Range. *J. Phys. Chem. B* **2012**, *116*, 1319–1327.
(29) Beudaert, P.; Lamare, V.; Dozol, J. F.; Troxler, L.; Wipff, G. Molecular Dynamics Simulations on Europium Nitrate Complexes with Neutral Organophosphorus Ligands. What Governs the Stoichiometry and Extractability of the Complex? *J. Chem. Soc., Perkin Trans. 2* **1999**, 2515–2523.
(30) Schurhammer, R.; Wipff, G. Effect of the TBP and Water on the Complexation of Uranyl Nitrate and the Dissolution of Nitric Acid into Supercritical CO_2. A Theoretical Study. *J. Phys. Chem. A* **2005**, *109*, 5208–5216.
(31) Cui, S. T.; de Almeida, V. F.; Khomami, B. In *Solvent Extraction: Fundamentals to Industrial Applications*; Proceedings of the ISEC 2008 Conference; Moyer, B. A., Ed.; Canadian Institute of Mining, Metallurgy and Petroleum: West Montreal, Quebec, Canada, 2008; pp 1069–1074.
(32) Ye, X. G.; Cui, S. T.; de Almeida, V. F.; Khomami, B. Interfacial Complex Formation in Uranyl Extraction by Tributyl Phosphate in Dodecane Diluent: A Molecular Dynamics Study. *J. Phys. Chem. B* **2009**, *113*, 9852–9862.
(33) Ye, X. G.; Smith, R. B.; Cui, S. T.; de Almeida, V. F.; Khomami, B. Influence of Nitric Acid on Uranyl Nitrate Association in Aqueous Solutions: A Molecular Dynamics Simulation Study. *Solvent Extr. Ion Exch.* **2010**, *28*, 1–18.
(34) Ye, X. G.; Cui, S. T.; de Almeida, V. F.; Hay, B. P.; Khomami, B. Uranyl Nitrate Complex Extraction into TBP/Dodecane Organic Solutions: A Molecular Dynamics Study. *Phys. Chem. Chem. Phys.* **2010**, *12*, 15406–15409.
(35) Cui, S. T.; de Almeida, V. F.; Hay, B. P.; Ye, X.; Khomami, B. Molecular Dynamics Simulation of Tri-*n*-butyl-Phosphate Liquid: A Force Field Comparative Study. *J. Phys. Chem. B* **2012**, *116*, 305–313.
(36) Available online at http://dasher.wustl.edu/tinker/distribution/params/amber99.prm.
(37) Wang, J.; Cieplak, P.; Kollman, P. A. How Well Does a Restrained Electrostatic Potential (RESP) Model Perform in Calculating Conformational Energies of Organic and Biological Molecules? *J. Comput. Chem.* **2000**, *21*, 1049–1074.

(38) Cornell, W. D.; Cieplak, P.; Bayly, C. I.; Gould, I. R.; Merz, K. M., Jr.; Ferguson, D. M.; Spellmeyer, D. C.; Fox, T.; Caldwell, J. W.; Kollman, P. A. A 2nd Generation Force-Field for the Simulation of Proteins, Nucleic-Acids, and Organic-Molecules. *J. Am. Chem. Soc.* **1995**, *117*, 5179−5197.
(39) Jorgensen, W. L.; Maxwell, D. S.; TiradoRives, J. Development and Testing of the OPLS All-Atom Force Field on Conformational Energetics and Properties of Organic Liquids. *J. Am. Chem. Soc.* **1996**, *118*, 11225−11236.
(40) Thomas, L. L.; Christakis, T. J.; Jorgensen, W. L. Conformation of Alkanes in the Gas Phase and Pure Liquids. *J. Phys. Chem. B* **2006**, *110*, 21198−21204.
(41) Ye, X.; Cui, S. T.; de Almeida, V. F.; Khomami, B. Effect of varying the 1−4 intramolecular scaling factor in atomistic simulations of long-chain N-alkanes with the OPLS-AA model. *J. Mol. Model* **2013**, *19*, 1251−1258.
(42) Dewar, M. J. S.; Thiel, W. Ground States of Molecules. 38. The MNDO Method. Approximations and Parameters. *J. Am. Chem. Soc.* **1977**, *99*, 4899−4907.
(43) Becke, A. D. Density-Functional Thermochemistry 3. The Role of Exact Exchange. *J. Chem. Phys.* **1993**, *98*, 5648−5652.
(44) Lee, C. T.; Yang, W. T.; Parr, R. G. Development of the Colle−Salvetti Correlation-Energy Formula into a Functional of the Electron-Density. *Phys. Rev. B* **1988**, *37*, 785−789.
(45) Bayly, C. I.; Cieplak, P.; Cornell, W. D.; Kollman, P. A. A Well-Behaved Electrostatic Potential Based Method Using Charge Restraints for Deriving Atomic Charges: The RESP Model. *J. Phys. Chem.* **1993**, *97*, 10269−10280.
(46) Bylaska, E. J.; W. A. de Jong; Kowalski, K.; ; Straatsma, T. P.; ; Valiev, M.; ; Wang, D.; ; E. Aprà; Windus, T. L.; ; Hirata, S.; ; Hackler, M. T. et al. *NWChem, A Computational Chemistry Package for Parallel Computers*, version 5.0, Pacific Northwest National Laboratory: Richland, WA, 2006.
(47) De Leeuw, S. W.; Perram, J. W.; Smith, E. R. Simulation of Electrostatic Systems in Periodic Boundary-Conditions 1. Lattice Sum and Dielectric-Constant. *Proc. R. Soc., London A* **1980**, *373*, 27−56.
(48) Allen, M. P.; Tildesley, D. J. *Computer Simulation of Liquids*; Clarendon Press, Oxford, 1987.
(49) Alejandrea, J.; Tildesley, D. J.; Chapela, G. A. Molecular Dynamics Simulation of the Orthobaric Densities and Surface Tension of Water. *J. Chem. Phys.* **1995**, *102*, 4574−4583.
(50) Tuckerman, M.; Berne, B. J.; Martyna, G. J. Reversible Multiple Time Scale Molecular Dynamics. *J. Chem. Phys.* **1992**, *97*, 1990−2001.
(51) Nosé, S. A Molecular Dynamics Method for Simulations in the Canonical Ensemble. *Mol. Phys.* **1984**, *52*, 255−268.
(52) Nosé, S. A Unified Formulation of the Constant Temperature Molecular-Dynamics Methods. *J. Chem. Phys.* **1984**, *81*, 511−519.
(53) Estok, G.; Wendlandt, W. W. Electric Moments of Some Alkyl Phosphates and Thiophosphates. *J. Am. Chem. Soc.* **1955**, *77*, 4767−4769.
(54) Petkovic, D. M.; Kezele, B. A.; Rajic, D. R. Dipole Moments of Some Neutral Organic Phosphates. *J. Phys. Chem.* **1973**, *77*, 922−924.
(55) http://webbook.nist.gov/chemistry/.